Precise and millidegree stable temperature control for fluorescence imaging: Application to phase transitions in lipid membranes

Elaine R. Farkas and Watt W. Webb
School of Applied and Engineering Physics, Cornell University, Ithaca, New York 14853, USA

(Received 23 June 2010; accepted 5 August 2010; published online 22 September 2010)

We present the design of a custom temperature-controlled chamber suitable for water or oil immersion fluorescence microscopy and its application to phase behavior in lipid bilayer vesicles. The apparatus is self-contained and portable, suitable for multiuser microscopy facilities. It offers a higher temperature resolution and stability than any comparable commercial apparatus, on the order of millidegrees. We demonstrate the utility of the system in the study of miscibility transitions in model membranes. The temperature-dependent phase behavior of model membrane systems that display liquid-ordered (L_o) phase coexistence with the liquid-disordered (L_d) phase is relevant to understanding the existence of heterogeneities in biological cell plasma membranes, ubiquitously termed "lipid rafts." © *2010 American Institute of Physics.* [doi:10.1063/1.3483263]

I. INTRODUCTION

Crucial information about phase behavior is found in the temperature dependence of various physical properties that define each phase. One family of methods that has been used extensively to characterize the physical properties of different phases in biological systems is fluorescence microscopy, which includes confocal, multiphoton, fluorescence lifetime, and polarization microscopy. The system described in this paper is applicable especially to biological specimens and measurements of temperature-dependent parameters in the vicinity of critical phase transition points, where high-temperature resolution and stability are necessary. We discuss this application to giant unilamellar vesicles (GUVs) labeled with phase-preferring fluorophores[1] visualized by laser scanning multiphoton microscopy (MPM). In lipid bilayer systems, there are several external parameters one could vary to observe phase transitions in multicomponent lipid bilayer vesicles, but in practice, it is easiest to control the temperature and composition instead of, for instance, the external pressure.

Compositional heterogeneity in the plasma membrane of eukaryotic cells was first discussed in the context of biological function by Simons and Ikonen.[2] These heterogeneities, which have since been shown to comprise a wide variety of spatial and temporal scales, are ubiquitously termed "rafts" and are often attributed to the differential miscibility of different membrane lipids.[3] Rafts have been implicated in such functions as protein sorting[2,4] and cell signaling.[4,5] Heterogeneities that are resistant to solubilization by nonionic detergents are postulated to have compositions similar to those of the liquid-ordered (L_o) phase found in model membranes,[4,6,7] while the surrounding matrix is thought to reside in the liquid-disordered (L_d) phase. The two phases are typically distinguished from one another by the extent of order in their acyl chains, although the exact definition of this order depends on the experimental apparatus used to measure it. The study of lipid phase behavior in bilayer systems is an important part of understanding the heterogeneous plasma membrane. Simple mixtures of at least three components[8,9] have been shown to exhibit liquid-liquid (L_o-L_d) immiscibility and have thus been used extensively as models of the cell membrane.

Temperature stability is important for the mapping of equilibrium phase diagrams; to observe miscibility transitions and reliably report on the behavior of the system, the temperature steps should be quasiadiabatic, slow enough that equilibrium is reestablished at each temperature increment. Temperature stability is even more important with respect to measurement of critical fluctuations in a system. Evidence suggests that biological membranes may tune their compositions to be near a miscibility critical point to exploit the divergent properties for biological functions,[10,11] or to be near a phase boundary to exploit sensitivity to compositional and temperature changes.[12] The idea that the cell membrane may exploit features of critical phenomena is not new,[13–16] and studies on both biological and model membranes have examined critical behaviors for insight into biological membrane functions.[16–22] Critical fluctuations in lipid composition have been linked to enzyme function[15,23] and to an anomalous increase in ion permeability.[13] The singular behavior of the diffusion coefficient has been associated with protein mobility[16] and environmental sensitivity.[24–26] It has been hypothesized that long-range protein-protein interactions may be due to the increase of the spatial scale of concentration fluctuations.[19,21] Critical mixing has been investigated theoretically with respect to the protein: lipid stoichiometry in membranes.[14,27] More recently, it has been proposed that critical fluctuations in the concentration of different lipids in both model[28,29] and plasma membranes[10] are what define lipid rafts. Thus, the biological applicability and the compendium of available information on lipid phase behavior make this an attractive system on which to demonstrate a new temperature-control apparatus.

There are two categories of temperature perturbations that can affect the observations of phase behavior: stationary

and nonstationary temperature gradients.[30,31] Detailed explanations and the equation governing these definitions can be found in Anisimov.[30] Stationary gradients are those that do not change within the characteristic relaxation time (or measurement time) of the system and thus may be thought of as spatial gradients with respect to the sample. Stationary temperature gradients are generally due to inhomogeneous heating or inhomogeneous heat dissipation. They lead to concentration[30,32,33] or density gradients[31] within the sample because a different equilibrium composition or density profile is established at each temperature. Away from a critical point, this may make the characterization of phase transitions difficult because the interfaces between the phases are no longer well defined. Near a critical point, concentration or density gradients induced by stationary temperature gradients have the effect of rounding off to a finite value of a theoretically divergent physical parameter.[30] There is also a broadening, or smearing out, of the "critical" regime of the critical anomaly with respect to temperature because there are now multiple critical points to consider, one for each composition (or density) band at each temperature. For stationary gradients, T_c will not be shifted to a new value. The relevance of such a scenario in lipid bilayer membrane systems has been discussed recently by Honerkamp-Smith *et al.*,[11] who state that a multicomponent system will have multiple critical points, although this assessment was with respect to genuine multicomponent systems and not nonequilibrated ones.

Nonstationary temperature perturbations describe those temperature changes that occur more quickly than the sample's characteristic relaxation time or the measurement time. Nonstationary gradients can be caused by inappropriately fast temperature jumps. Both near and away from critical points, these gradients lead to nonequilibrium conditions in experiments and increase the random error. An example of errors incurred by nonequilibrium conditions is superheating or supercooling samples and ascribing the wrong phase area (volume fractions) to a given composition at a given temperature. We have observed such phenomena firsthand in our lipid research: for some lipid compositions, cooling vesicles too quickly lead to the observation of homogeneous vesicles rather than phase separated vesicles, because some phases (viscous gels and L_o phases) require significant time to nucleate and grow.[34] The effects of nonstationary gradients are more likely near the critical point, because the sample relaxation times become increasingly large. Additionally, nonstationary gradients may lead to shifts in the observed T_c. Such a shift could lead to improper determination of critical exponents if not properly accounted for with renormalized exponents. The extent of this effect is often dependent on the physical parameter being observed. For example, it was demonstrated experimentally that the critical temperature for xenon differed depending on whether the thermal relaxation time or the heat capacity at constant volume was measured.[35] The wrong choice of T_c, in this case as the temperature of maximum C_v, led to an erroneous calculation of the critical exponent because the measurement of C_v was much more susceptible to perturbations due to gravity than, for example, a measurement of the thermal relaxation time.[30]

II. APPARATUS

The overall design of the sample bath was derived from principles first used in this laboratory over three decades ago to observe continuous phase transitions (i.e., critical phenomena) in sulfur hexafluoride.[36,37] Our apparatus was designed to minimize spatial and temporal temperature gradients while maintaining accessibility to the sample and portability of the sample bath. This is challenging in the environment of a light microscope due to the need to accommodate the imaging equipment and prevent heat loss while maintaining a relatively open system. An appropriate sample bath should be small enough to accommodate the commercial microscope without compromise of user access or movement of the microscope stage, but well insulated enough to prevent heat loss. Imaging of biological materials often requires water or oil immersion lenses in which the immersion medium directly contacts the sample; thus, the metal-cased objective lens will act as a heat sink if it is not properly countered. Many of the sample container materials such as glass coverslips and thin polycarbonate plastic Petri dishes used in traditional biological imaging also dissipate heat fairly efficiently.

A diagram of the basic elements of the imaging pathway and the sample bath is depicted in Figs. 1(a) and 1(b). The sample bath consisted of a cylindrical Teflon [polytetrafluoroethylene (PTFE)] cup with approximately 1/8 in. thick walls. The inner diameter (ID) of the cup is 2.25 in. and the height is 2.00 in. The cup was filled with water for the bath medium, since this is the immersion medium for the objective lens (UPLAN APO infinity-corrected 60×, Olympus, Pennsylvania, USA) we used. A hole was bored through the bottom of the cup through which a portion of the objective lens was inserted. A nitrile o-ring was situated between the Teflon and the lens to prevent leakage of the bath material (water). A small groove was cut into the sidewall of the borehole in the Teflon cup to accommodate compression of the o-ring without slippage. When all elements (heaters, sample holder, and thermometers) were assembled inside the chamber for imaging, the top portion was sealed from the atmosphere with flexible adhesive foam to prevent heat loss and water evaporation.

That the immersion medium for the lens is water is fortunate, because its high specific heat makes it excellent thermal bath material: the more water surrounding the sample, the more difficult it is energetically to change the temperature, thus guarding against fluctuations and gradients. The bath described here accommodates roughly 100 ml water. Note that a similar design could also be used with lens immersion oil. The change in refractive index of the lens glass, as well as the water, with temperature can be compensated for by using an objective with a corrective collar, as we have done. The changes are generally quite small for the temperature ranges considered here, ~20–50 °C. For example, at 1.0 bar pressure and a wavelength of 589.32 nm, the index of refraction of water changes from 1.332 83 to 1.328 92 when the temperature changes from 20 to 50 °C, respectively.[38]

The sample is placed into the bath by an external sample holder. This holder is composed of a copper "chamber" and a

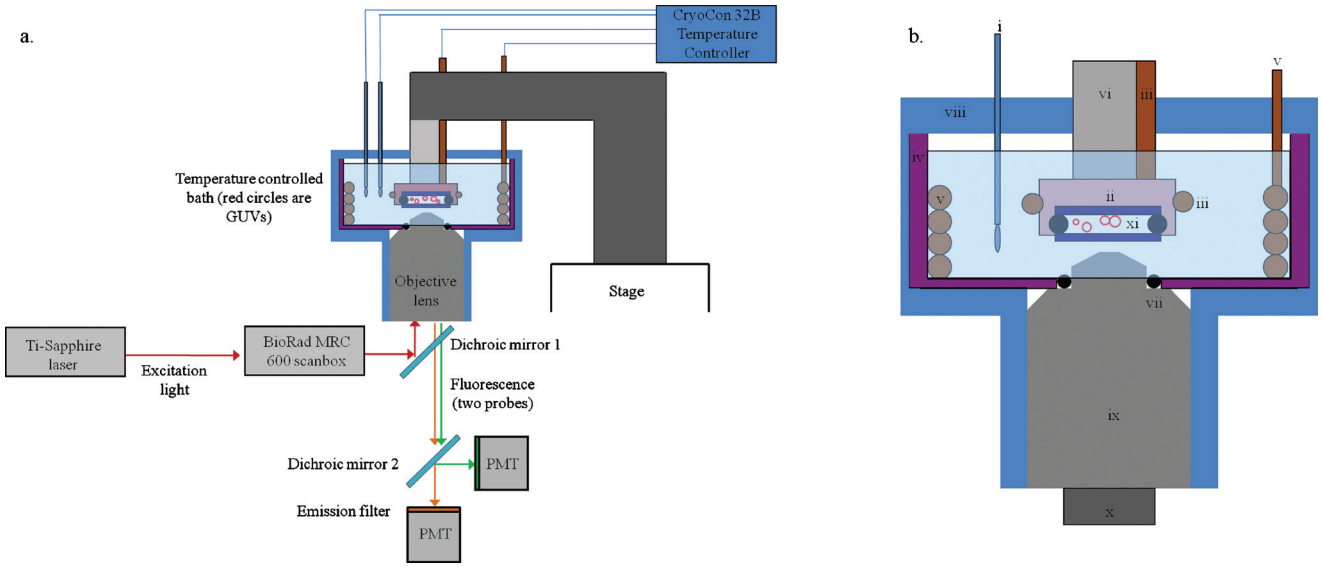

FIG. 1. (Color) (a) Block diagram of the imaging apparatus. 780 nm excitation light (red arrow) from a Ti:sapphire laser is routed to a Bio-Rad MRC600 scanbox, which raster scans the beam through the objective lens and across the sample. The sample consists of an aqueous suspension of GUVs (red circles) between two glass coverslips (dark blue) and sealed from the bath water by clear nail polish and Fomblin perfluorinated vacuum grease. The entire sample and part of the objective lens are contained within the sample bath and submerged in water as shown. Two heaters (orange) and two RTD thermometers (one for each heater) are connected to the CryCon model 32B temperature controller, which is remotely operated by an RS232 connection to a PC. The excitation light is separated from the fluorescence light (orange and green arrows, denoting two different fluorophores) by dichroic mirror 1, and the fluorescence emissions are then separated by color by dichroic mirror 2 before being collected by the PMTs. (b) Close-up of the sample bath. The components are labeled i–xi: (i) Pt100 RTD, (ii) copper sample holder, (iii) small (loop 2) cable immersion heater, (iv) Teflon cup (purple), (v) large (loop 1) bath water heater, (vi) Teflon rod for the sample holder, (vii) o-ring seal (black) between objective lens and Teflon cup, (viii) foam insulation (blue), (ix) objective lens (UPlan Apochromat 60×, Olympus), (x) thermal isolator for objective lens, and (xi) GUV (red circles) samples between two round coverslips (dark blue).

Teflon rod. The portion of the sample holder directly in contact with the sample is the copper chamber. The copper piece is cylindrical, 5/8 in. high, and 9/10 in. in diameter. One side of the copper piece is tapped to a depth of 1/4 in. inside. This copper piece, along with a portion of the Teflon rod, is completely submerged in water when the bath is operational. The Teflon rod is roughly 2 3/8 in. long and 5/8 in. in diameter and is threaded on one end that screws into the copper piece. The Teflon rod acts as a thermal isolator and is attached to a rigid aluminum platform that is securely fastened onto the microscope stage, as depicted in Fig. 1(a). Comparable commercial systems, such as the model TS-4 (Physitemp, New Jersey, USA), the Biostage 600 (20/20 Technology Inc., North Carolina, USA), or the HE-200 stages (Dagan Corp., Minnesota, USA), as well as custom systems based on Peltier heating elements,[10,29,39,40] use air or metal to transfer heat and maintain the temperature. Both air and metals have considerably lower heat capacities than water and are thus more likely to experience heat loss and corresponding temperature gradients; note that the stability for each of three systems cited is $\pm 0.1\ ^{\circ}\mathrm{C}$.

Temperature control of the sample bath was implemented by two independent proportional-integral-derivative (PID) loops, with one heater (zone) per loop. The power supply for both of the heaters was the CryoCon model 32B temperature controller (CryoCon, California, USA). This controller was selected because it has very stable current outputs over three decades of power; thus a wide range of temperatures can be accessed with uncompromised stability, provided the overall design is properly insulated. Both outputs of the 32B are linear current supplies. The larger heater in loop 1 used the 50 W, 50 Ω radio frequency interference (RFI) filtered output while the small heater in loop 2 used the 10 W, 50 Ω output.

Loop 1 was used to heat the bulk of the water in the bath, and loop 2 was used to maintain a stable temperature at the copper sample holder. In loop 1, heating was accomplished by a 0.125 in. [outer diameter (OD)] immersion cable immersion heater (Watlow, Missouri, USA) coiled to fit snugly to the inner perimeter of the Teflon cup such that the coil dimensions were 1.95 in. (ID) by 2.25 in. (height). A cable heater is a long cylindrical metal element coated such that it is submersible in liquid without shorting. A 2.0 in. "dead" element, which emits no heat, was included at the top portion of the heater that sticks up and out of the top of the cup; this prevents heat loss and ensures that only the hot portion of the heater was submerged. This heater was used for equilibrium measurements, such as measuring the phase transition temperature. The heater in the second control loop consisted of a smaller cable immersion heater (Watlow). Its end was curled to make a coil such that it wrapped around the circumference of the copper piece, as shown in Fig. 1. This smaller heater was 0.094 in. in diameter and 8.25 in. in length. Like the large heater in loop 1, the one in loop 2 also contained a 2.0 in. dead element. The model 32B was also used to measure the temperature, with one probe per control loop. Temperature was monitored with calibrated platinum resistance temperature devices (RTDs, 100 Ω, 1/10 DIN (Deutsches Institut für Normung), Alltemp Sensors, Texas, USA). The probe for loop 1 was situated such that it was 0.50 in. from the bottom of the Teflon cup. The probe for loop 2 was mounted directly to the Teflon rod such that its tip

contacted the copper sample chamber. Direct access to the sample by the probe was not possible because the sample is sealed from the surrounding bath water. For application to measurements of phase transitions and critical phenomena described here, the RTD was the preferred probe because it has the best stability and accuracy near room temperature; selection of appropriate temperature probes is reviewed in Tong.[41]

III. OPTICAL APPARATUS

Samples were visualized using MPM. Briefly, 780 nm, 200 fs pulsed excitation light from a titanium sapphire Tsunami laser (Spectra-Physics, California, USA) was used to excite two fluorescent probes with different emission wavelengths simultaneously in the GUV samples. The excitation light was sent to a galvanometrically controlled MRC600 x-y scanner (BioRad, California, USA), which scans the beam across the sample, and through the microscope to the GUV sample. An inverted Zeiss Axiovert 135 microscope (Carl Zeiss GmbH, Germany) is used for all studies. Fluorescence emissions are collected in nondescanned mode by external gallium arsenide phosphate photomultiplier tubes (Hamamatsu, New Jersey, USA). Fluorescence emissions and images were separated into blue and red channels by a dichroic mirror (Chroma Technologies, Vermont, USA). Emission filters (Chroma) were placed in front of the photomultiplier tubes (PMTs) to isolate the color for each channel: 490 (nm) short pass filter for the blue channel and 600/90 bandpass filter for the red channel.

IV. LIPIDS AND GUV PREPARATION

Dioleoylphosphatidylcholine (DOPC), stearoyl sphingomyelin (SSM), cholesterol, and the probe lissamine-rhodamine dipalmitoylphosphatidylethanolamine (LR-DPPE) were purchased from Avanti Polar Lipids (Alabama, USA) and used without further purification. The probe naphthopyrene was purchased from Sigma Aldrich (Missouri, USA). Lipids, cholesterol, and probes were dissolved in chloroform, and the lipid concentration in chloroform solutions was determined using the microphosphorus assay.[42] Vesicles were prepared according to the electroformation procedure described in Ayuyan and Cohen,[43] which was modified from that described by Angelova *et al.*[44] The details of the exact procedure are described in Morales-Penningston *et al.*[34] For imaging, aqueous suspensions of GUVs were placed between two round glass coverslips separated by Fomblin perfluorinated grease and sealed by clear nail polish. This "sandwich" was then mounted onto the copper sample holder by three clips attached to the bottom of the holder.

Lipid phase behavior was observed using fluorescent probes. Fluorophores partition into different lipid phases depending on their structures.[1] If two dyes prefer different phases and emit at different wavelengths, the lipid phases are observed as two distinct colors, as depicted in Fig. 2 for SSM/DOPC/cholesterol=0.23/0.27/0.50. For the data presented here, the false red color indicated the L_d preferring probe LR-DPPE and the false blue color indicated the L_o preferring probe naphthopyrene.

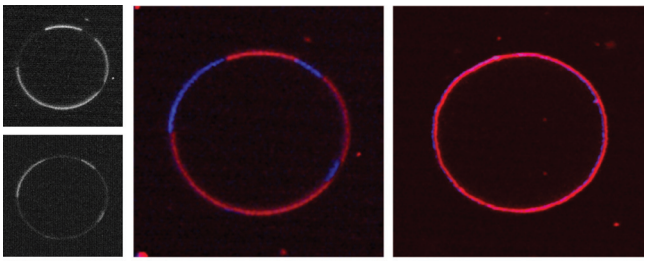

FIG. 2. (Color) Dye partitioning and phase transition in a GUV. For this sample, SSM/DOPC/cholesterol=0.23/0.27/0.50. The black and white images depict the two different fluorescence channels at 24.600 °C prior to merging and false color assignment. The upper black-and-white image shows the LR-DPPE fluorescence (L_d phase) and the lower image shows naphthopyrene fluorescence (L_o phase). The middle image shows an equatorial section of a GUV with L_o-L_d phase coexistence at 24.600 °C and the right image shows the GUV at 35.300 °C, after it has undergone a miscibility transition. The red false color denotes the L_d phase probe LR-DPPE and the blue false color denotes the L_o phase probe naphthopyrene.

V. DATA COLLECTION

Profiles of temperature versus time were captured using remote operation of the temperature controller. The controller was connected to a PC via an RS232 connection, and the temperature was sampled at 5 s intervals. The CRYOCON UTILITY software provided with the instrument was used for remote instrument control. The data were then exported to a spreadsheet and plotted.

The standard deviations from a set of temperature versus time data are reported as the stability limits of the temperature bath. Unless otherwise noted, the standard deviations reported are for individual runs, not multiple data sets.

To observe phase transitions, 100 ml of de-ionized water was added to the sample bath. The sample holder, RTDs, and heaters were submerged and the heaters were then slowly ramped from 22.000 °C to higher temperatures to determine the miscibility temperature; the ramp rate was 0.010 °C/min or slower in order to avoid superheating the sample. The morphology and dye partitioning were checked at roughly every 2–5 °C until miscibility was observed between the two phases, at which point the vesicle appeared homogeneous in the two fluorescence channels. An example of a miscibility transition is depicted in Fig. 2. Below the transition temperature, merged images from each fluorescence channel depict two distinct colors (phases), whereas above the transition temperature, the vesicle is homogeneous in both channels.

VI. TEMPERATURE STABILITY/PERFORMANCE

Temperature versus time plots for fixed locations in the sample chamber is depicted in Fig. 3 for four different set-point temperatures. One can see that for a fixed probe location in the sample bath, the temperature is very stable for various set-point temperatures ranging from 30.000 to 45.000 °C on the time scale of hours: the overall standard deviation of fluctuations in the measured temperature is on the order of millidegrees. This number was obtained by a simple average of the all the data points for a given run, and it is depicted both as error bars and as the numerical standard

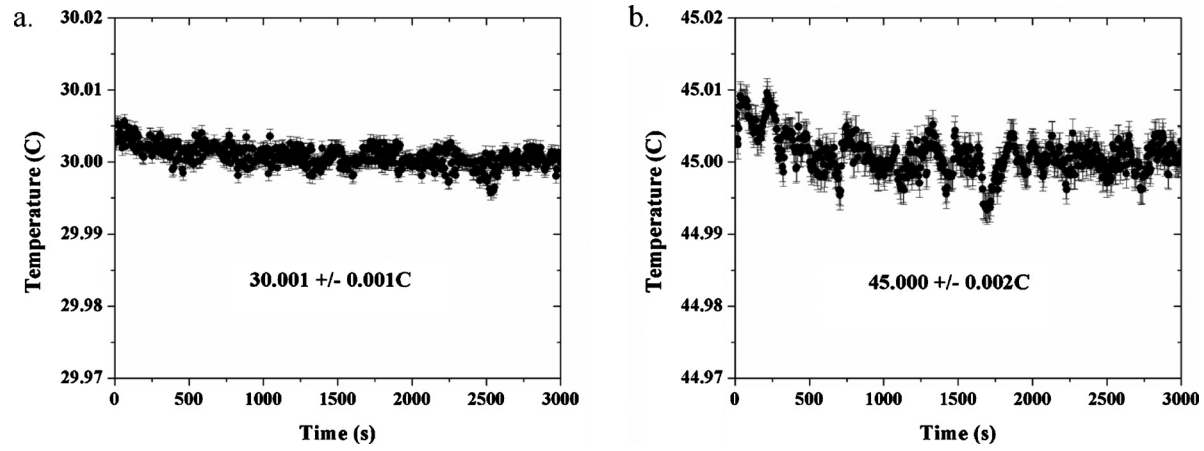

FIG. 3. Temporal stability of the temperature for a fixed location in the sample bath. The sample temperature at a fixed location is stable to within milli-Kelvins of the set-point temperature for periods of hours. The temperatures displayed in the insets are the recorded temperatures; the set point temperatures were (a) 30.000 °C and (b) 45.000 °C. Each graph depicts one run only; thus, the error bars depicted on the graphs for the actual temperature (vs setpoint temperature) refer to the standard deviations of time averages of the temperature readings. Therefore, all are the same in length for a given data set.

deviation from the recorded temperature in Fig. 3. The sample bath was also designed to minimize convection and spatial temperature gradients and to maximize the temporal temperature stability at the sample. Spatial temperature gradients are observed by measuring the temperature at two or more locations within the sample or sample chamber. This can be done using two probes simultaneously (provided they are interchangeable), or with the same probe at different locations. In these experiments, the latter option was used.

To measure the gradients in the plane of the sample, the RTD was placed at locations 1 cm apart on either side of the sample chamber, at a constant depth in the water. The temperature was recorded at 5 s intervals by an RTD via remote operation the temperature controller from a PC. Two recordings were made at each location and the data at each time point were averaged. The recordings at a set point of 32.000 °C are depicted in Fig. 4(a). The average gradient was $1 \times 10_{-6}$ °C/μm, or roughly 0.000 25 °C across a distance of 225 μm; this length is the width of the field of view at a zoom equal to 1.0 for the MPM apparatus used in these experiments. To check for gradients in the vertical (optical axis) direction, the probe was placed at locations 3 cm apart in the sample bath and the results are depicted in Fig. 3(b). Here, the gradient is more dramatic: $8.1 \times 10_{-6}$ °C/μm. For a sample roughly 150 μm thick (the area between the two glass coverslips where the vesicles reside), this translates into a vertical gradient of 0.001 °C over the entire chamber thickness. The graphs are an average of two measurements and the error bars at each data point are a combination of the standard deviation between two measurements and the standard deviation of the average of all time points for a data set.

VII. PHASE DIAGRAM

The temperature-dependent, quasiternary phase diagram is depicted in Fig. 5(a). The samples used to prepare this

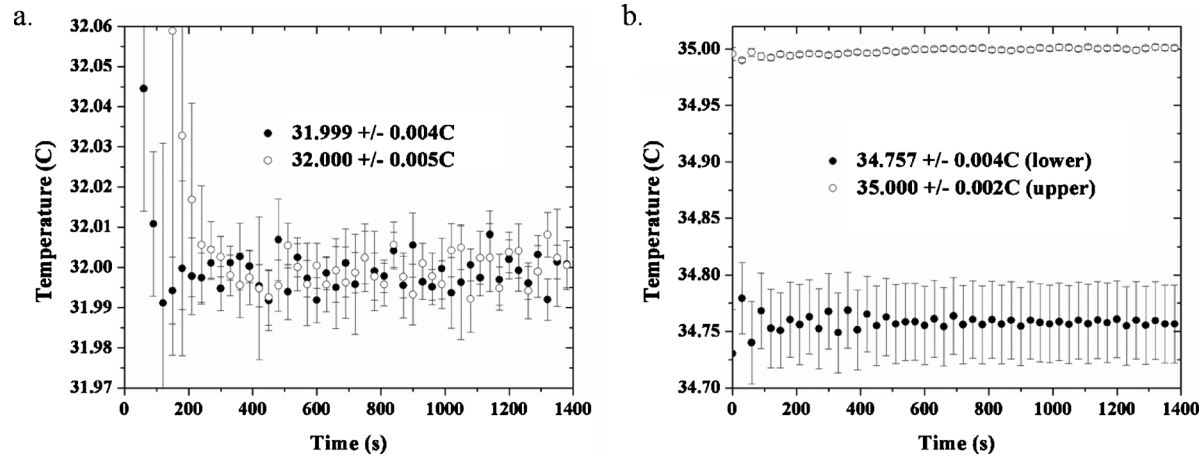

FIG. 4. Spatial temperature gradients. The open circles and black circles refer to the two different locations. (a) Measurement of the temperature vs time at positions 1 cm apart, at a constant depth in the sample chamber (set point of 32.000 °C). (b) Measurement of the temperature at different depths in the sample chamber, 3 cm apart. Each open circle or black circle data point is an average of two measurements. For a given plot, the error bars represent a combination of the standard deviation of two data sets used to produce the depicted averaged plot and the time average of the temperature readings for the averaged plot. It should be noted that the data were recorded at 5 s intervals, but those displayed on the graphs have been made sparse (30 s intervals instead of 5 s intervals) for the sake of clarity.

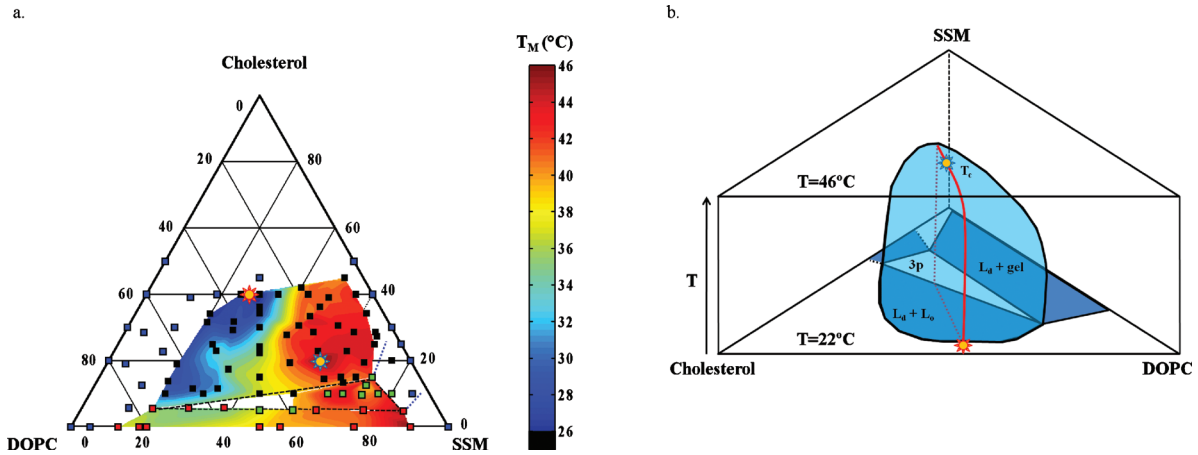

FIG. 5. (Color) Temperature-dependent ternary diagram for cholesterol/SSM/DOPC. (a) Ternary diagram. Color denotes miscibility transition temperatures as indicated by the scale to the right, and the coexistence boundaries for the colored regions are for 22.000 °C. Blue points refer to one-phase samples at 22.000 °C, black points to L_o-L_d coexistence at 22.000 °C, red points to gel-L_d coexistence at 22 °C, and green points to three-phase samples at 22.000 °C, as observed using two-photon microscopy. The red star denotes the critical point at 22.000 °C and the blue star denotes the overall critical point at 46.004 ± 1.500 °C. (b) A schematic of the L_o-L_d coexistence region with the line of critical points (red) extending from the point at 22 °C to the upper critical point T_c at 46.004 °C.

diagram were prepared and observed under anaerobic conditions in order to minimize lipid oxidation. Sample points displaying two-phase coexistence are colored blue (L_o-L_d) and red (L_d-gel); sample points appearing optically homogeneous are black; and sample points displaying three-phase coexistence are green. The colored contours indicate the miscibility transition temperatures of the compositions inside the miscibility gaps, which, at 22.000 °C, are denoted by solid lines. In other words, the phase boundaries at 22.000 °C are where the colored region ends. The L_o-L_d coexistence region extends very close to the SSM-cholesterol binary axis. Temperature measurements were not recorded in the region of <5 mol % DOPC because the L_d domains consistently bulged outward and budded off of the parent vesicles, even with osmotic swelling of the GUVs. Thus, the right (high SSM) side of the miscibility gap for L_o-L_d coexistence at 22.000 °C depicted in Fig. 5(a) is not very accurate. The three-phase region is denoted by the triangle circumscribed by the black dashed line. The dashed blue lines indicate the two-phase region of L_o-gel coexistence that theoretically must be present[45] but was not directly or unambiguously observed using optical microscopy. Note that this region does not have to touch the binary cholesterol-SSM axis as drawn; in theory, it could instead form a closed loop without touching a binary axis, like the L_o-L_d coexistence region at 22.000 °C. The stars denote critical points, the uppermost of which (at 46.004 ± 1.500 °C) is depicted by the blue-lined star. Figure 5(b) depicts an approximate 3D view of the L_o-L_d coexistence region, with temperature as the third axis. In this figure, the composition axes are rotated with respect to those in Fig. 5(a).

The experimental deviations in transition temperatures for a given average composition ranged from 0.800 to 5.000 °C; a higher degree of variation in the observed T_M's for a given composition was observed with increasing SSM content and with decreasing cholesterol content and was thus especially prevalent in vesicles containing a gel phase. These variations may be due to slight differences in the vesicle compositions within a given sample, to thermal gradients in the sample chamber, or to kinetic effects. The latter are especially important in vesicles where the phases have a markedly different viscosity.

VIII. QUENCH MEASUREMENTS

Two versions of the sample bath were developed. The first was described in Sec. II and was used for measurement of equilibrium properties observed by MPM. The second design, described here, was used for the measurement of kinetic phenomena (quenches) observed in real time by wide-field illumination. Quench measurements refer to those in which the temperature of the bath is rapidly dropped in order to observe nonequilibrium (or "kinetic") phenomena. Kinetic properties can provide an important complement to equilibrium (quasiadiabatic) studies of phase behavior. For example, the morphology of phase separation and the time-dependent domain growth can vary as functions of system dimensionality, or of whether the order parameter is conserved or not, or on hydrodynamics (such as whether the surface tension competes with viscous or inertial forces). Thus, kinetic information could be used to help distinguish between appropriate models for a complex system such as the phase separated bilayer.

For nonequilibrium measurements, a high temperature is first reached using both the large and small heaters, and one of the recirculating water baths. The temperature is typically above the miscibility transition temperature for two lipid phases, such that quasi-instantaneous quenching will produce phase separation. The main differences between the two types of baths were the type of heater used in loop 1 (thermostatted copper tubing for the quench bath type or an immersion coil for the equilibrium bath type), the type of probe used to measure temperature (type T thermocouple for the quench bath type or RTD for the equilibrium bath type), and the type of detectors used to image the sample [integrated charge-coupled device (ICCD) or electron multiplying

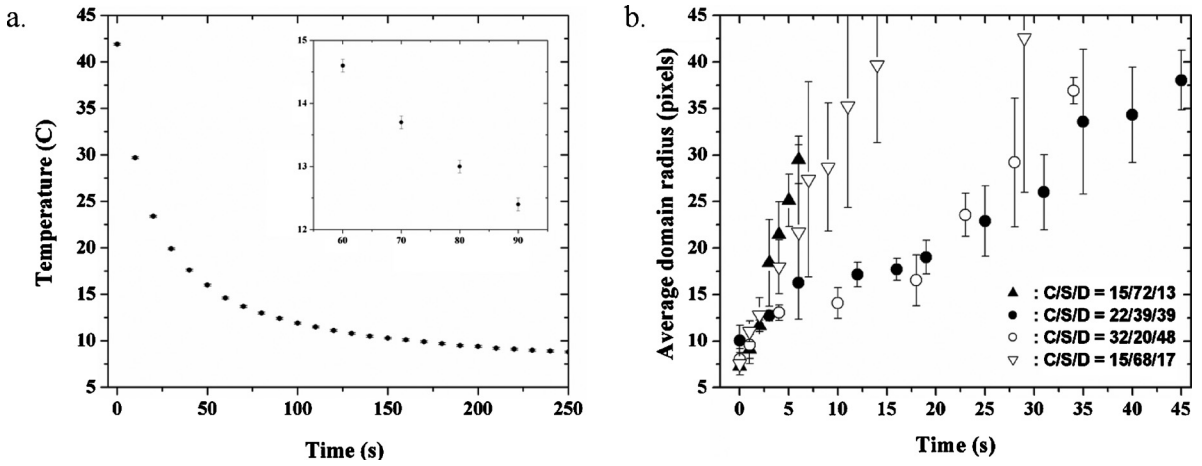

FIG. 6. Quench data. (a) An example of the temperature (°C) reading near the sample vs time (second) for a quench experiment. The inset shows the error bars up close. (b) Average domain radius (pixels) vs time (second) for four different compositions quenched below the L_o-L_d miscibility gap. The error bars in (a) reflect the uncertainty in the thermometer (±0.1 °C) only; thus, they are of constant length for all data points. The error bars depicted in (b) reflect the standard deviations of the sample averages.

charge-coupled device (EMCCD) for real-time image capture in the quench bath type or PMT for the equilibrium bath type]. Moreover, quenched sample had to be illuminated using wide-field illumination instead of scanned laser illumination. This was accomplished by a mercury arc lamp built into the microscope. Additionally, a second bath had to be used for rapid temperature change as described below.

For quenches, the temperature at the copper holder was monitored using a polyurethane insulated type T IT-24P thermocouple (Physitemp, New Jersey, USA) connected to a thermometer separate from the BAT-10 thermometer controller (Physitemp). The recirculating water bath had its own PID controls independent of the temperature controller as well as its own platinum RTD. For the kinetic experiments, however, a thermocouple was necessary to measure the extremely fast quenches, as RTDs in general have a much slower response time.

The loop 1 heater was copper tubing, thermostatted externally by a recirculating NESLAB RTE 221 water bath (Thermo Fisher Scientific, Massachusetts, USA). In this type of heating process, thermostatted water was pumped through 1/8 in. ID copper tubing in a closed line. This copper tubing was tightly coiled and placed inside the PTFE sample bath in the same manner as the immersion cable heater [Fig. 1(b), v]. The copper tubing only spanned the height of the Teflon cup; the input and return to the recirculating bath were made of plastic tubing wrapped in thermally insulating foam. Outside of the sample chamber, the input and output tubing were coupled via a Teflon three-way valve to an additional recirculating water bath held at a much lower temperature (4.00 °C typically). Quenching is accomplished when the smaller second heater is turned off and the thermostatted water supply is switched from the high temperature recirculating bath to the bath held at 4.00 °C. The quench was relatively instantaneous, as depicted in Fig. 6(a). The error bars in Fig. 6(a) reflect the uncertainty imparted by the thermometer, ±0.1 °C; thus, they are constant at each data point. The data are for one run only.

For each of four compositions, the temperature was quenched from 41.0–43.0 to 20.0 °C in roughly 45 s. The radii of domains (in units of pixels) as functions of time (in seconds) were then recorded and are depicted in Fig. 6(b). The variation reflected in the error bars was due to variations of the domain radii at a given time. It is obvious from Fig. 6(b) that there are at least two different regimes of domain growth kinetics with respect to composition: the red and green curves, for cholesterol/SSM/DOPC=0.15/0.72/0.13 and 0.15/0.68/0.17, respectively, comprise the "fast" regime, and the black and blue curves, for 0.22/0.39/0.39 and 0.32/0.20/0.48, respectively, comprise a "slow" regime. The domain radius versus time data depicted in Fig. 6 can be fitted according to known domain growth laws for which $R(t) \sim t_n$ (where R is the domain radius). When these data were plotted on a log-log plot and fit to a linear equation, the result was that the fast regime samples had an exponent of 0.96 ± 0.26 and the slow regime samples, for $t > 10$ s, had an exponent of 0.64 ± 0.06.

IX. OUTLOOK

Peltier heaters are more commonly used than resistance heaters for temperature control in the biological sciences. These heaters have been used successfully for temperature controlled microscopy in both "homebuilt" set-ups[10,29,39,40] and commercial set-ups such as the PhysiTemp T4 for stabilities of ±0.1 °C. However, this could be improved by using water as the heat bath and heat transfer material, as we have done in this study. Using a Peltier device to heat the sample bath water may be more desirable than using resistance heaters due to the ability to cool the sample in a controlled manner as well as heat it. For equilibrium studies here, cooling was achieved by setting the set point temperature to a lower value and allowing the very slow equilibration with the surroundings. An improved design would have a cylindrically arranged array of Peltier devices encased and sealed within a waterproof cylinder. The cylinder should be made of a lightweight conductor of heat such as aluminum. This cylinder would replace the PTFE sample cup in the

current system so that the immersion coils or thermostatted copper tubing would be unnecessary. Another improvement would be to position the RTD closer to the sample. This would likely require a smaller RTD than the wire-wound variety we currently use, such as a platinum thin film RTD (Minco, Minnesota, USA). Unfortunately, commercially available film RTDs have thus far not been designed to be submersible in liquid baths. The ability to reach higher temperatures may be desired by some researchers as well. The main parameter preventing this is the lack of water immersion objective lenses with high-temperature capabilities. Most water immersion objective lenses can only be used up to about 55 °C.

X. CONCLUSION

The design presented here, capable of millidegree stability in both space and time, is one of the most stable and accurate when compared with similar commercial and custom built designs described in the literature. The justifications for this level of temperature control were delineated in the introduction, namely that quantitative analysis of critical phenomena in the form of critical exponents requires this level of resolution, and that observation of noncritical miscibility transitions for quasiequilibrium conditions requires the elimination of temperature gradients. The apparatus was successfully applied to imaging miscibility transitions in a ternary lipid system which displays L_o-L_d phase coexistence. The phase diagram was subsequently mapped out with respect to temperature and composition and is depicted in Fig. 5.

A temperature-controlled sample bath suitable for optical microscopy was presented. The sample chamber design depends intimately on the system and the type of measurement desired.

It insulated the sample from the environment to maintain adiabaticity for measurements of equilibrium parameters, and it was heated uniformly in the vicinity of the sample to avoid temperature gradients and convection of the bath. A constant temperature bath surrounded the sample because the heater could not be placed directly on the sample. All of these considerations led to the development of a bath that was stable and accurate to a few millidegrees.

ACKNOWLEDGMENTS

The authors would like to thank Gerald W. Feigenson and Tobias Baumgart for helpful discussions, and Mark A. Williams for editorial assistance. This research was supported in part by the STC Program of the National Science Foundation under Agreement No. ECS-9876771 and by NSF Grant No. CHE-0242328 and by NIH-NIGMS training Grant No. GM08267.

[1] T. Baumgart, G. Hunt, E. R. Farkas, W. W. Webb, and G. W. Feigenson, Biochim. Biophys. Acta–Biomembranes **1768**, 2182 (2007).
[2] K. Simons and E. Ikonen, Nature (London) **387**, 569 (1997).
[3] A. Rietveld and K. Simons, Biochim. Biophys. Acta–Rev. Biomembranes **1376**, 467 (1998).
[4] R. E. Brown and E. London, J. Biol. Chem. **275**, 17221 (2000).
[5] E. D. Sheets, D. Holowka, and B. Baird, Curr. Opin. Chem. Biol. **3**, 95 (1999).
[6] J. H. Ipsen, G. Karlström, O. G. Mouritsen, H. Wennerström, and M. J. Zuckermann, Biochim. Biophys. Acta–Biomembranes **905**, 162 (1987).
[7] A. V. Samsonov, I. Mikhalov, and F. S. Cohen, Biophys. J. **81**, 1486 (2001).
[8] C. Dietrich, L. A. Bagatolli, Z. N. Volovyk, N. L. Thompson, M. Levi, K. Jacobson, and E. Gratton, Biophys. J. **80**, 1417 (2001).
[9] S. L. Veatch and S. L. Keller, Biophys. J. **85**, 3074 (2003).
[10] S. L. Veatch, O. Soubias, S. L. Keller, and K. Gawrisch, Proc. Natl. Acad. Sci. U.S.A. **104**, 17650 (2007).
[11] A. R. Honerkamp-Smith, S. L. Veatch, and S. L. Keller, Biochim. Biophys. Acta–Biomembranes **1788**, 53 (2009).
[12] G. W. Feigenson, Annu. Rev. Biophys. Biomol. Struct. **36**, 63 (2007).
[13] S. Doniach, J. Chem. Phys. **68**, 4912 (1978).
[14] F. Jahnig, Biophys. J. **36**, 347 (1981).
[15] A. Raudino, Eur. Phys. J. B **2**, 197 (1998).
[16] A. J. Jin, M. Edinin, R. Nossal, and N. L. Gershfeld, Biochemistry **38**, 13275 (1999).
[17] A. Mitaku, T. Jippo, and R. Kataoka, Biophys. J. **42**, 137 (1983).
[18] A. Ruggiero and B. Hudson, Biophys. J. **55**, 1111 (1989).
[19] E. Sackmann, *Handbook of Biological Physics* (Elsevier, St. Louis, MO, 1995).
[20] S. Halstenberg, W. Schrader, P. Das, J. K. Bhattacharjee, and U. Kaatze, J. Chem. Phys. **118**, 5683 (2003).
[21] A. Celli, S. Beretta, and E. Gratton, Biophys. J. **94**, 104 (2008).
[22] M. C. Heinrich, I. Levental, H. Gelman, P. A. Janmey, and T. Baumgart, J. Phys. Chem. B **112**, 8063 (2008).
[23] P. Girard, J. Prost, and P. Bassereau, Phys. Rev. Lett. **94**, 088102 (2005).
[24] J. Prost, J. B. Manneville, and R. Bruinsma, Eur. Phys. J. B **1**, 465 (1998).
[25] Y. Tserkovnyak and D. R. Nelson, Proc. Natl. Acad. Sci. U.S.A. **103**, 15002 (2006).
[26] M. Haataj, Phys. Rev. E **80**, 020902 (2009).
[27] Z. Zhang, M. M. Sperotto, M. J. Zuckermann, and O. G. Mouritsen, Biochim. Biophys. Acta–Biomembranes **1147**, 154 (1993).
[28] A. R. Honerkamp-Smith, P. Cicuta, M. D. Collins, S. L. Veatch, M. den Nijs, M. Schick, and S. L. Keller, Biophys. J. **95**, 236 (2008).
[29] J. Juhasz, F. J. Sharom, and J. H. Davis, Biochim. Biophys. Acta–Biomembranes. **1788**, 2541 (2009).
[30] M. A. Anisimov, Sov. Phys. Usp. **17**, 722 (1975).
[31] A. V. Voronel, *Phase Transitions and Critical Phenomena* (Academic, New York, 1976).
[32] Y. R. Chashkin, V. G. Gorbunova, and A. V. Voronel, Sov. Phys. JETP **22**, 304 (1966).
[33] Y. P. Blagoi, V. I. Sokhan, and A. A. Pavlichenko, JETP Lett. **11**, 190 (1970).
[34] N. F. Morales-Penningston, J. Wu, E. R. Farkas, S. L. Goh, T. M. Konyakhina, J. W. Zheng, W. W. Webb, and G. W. Feigenson, Biochim. Biophys. Acta–Biomembranes **1798**, 1324 (2010).
[35] C. Edwards, J. A. Lipa, and J. M. Buckinham, Phys. Rev. Lett. **20**, 496 (1968).
[36] E. S. Wu and W. W. Webb, Phys. Rev. A **8**, 2065 (1973).
[37] E. S. Wu and W. W. Webb, Phys. Rev. A **8**, 2077 (1973).
[38] I. Thormahlen, J. Straub, and U. Grigull, J. Phys. Chem. Ref. Data **14**, 933 (1985).
[39] L. D. Chabala, R. E. Sheridan, D. C. Hodge, J. N. Power, and M. P. Walsh, Pfluegers Arch. Eur. J. Physiol. **404**, 374 (1985).
[40] S. L. Nail, L. M. Her, C. P. B. Proffitt, and L. L. Nail, Pharm. Res. **11**, 1098 (1994).
[41] A. Tong, Sens. Rev. **21**, 193 (2001).
[42] P. B. Kingsley and G. W. Feigenson, Chem. Phys. Lipids **24**, 135 (1979).
[43] A. G. Ayuyan and F. S. Cohen, Biophys. J. **91**, 2172 (2006).
[44] M. I. Angelova, S. Soléau, Ph. Méléard, F. Faucon, and P. Bothorel, Prog. Colloid Polym. Sci. **89**, 127 (1992).
[45] M. E. Fisher and Y. C. Kim, J. Chem. Phys. **117**, 779 (2002).